Coupled dam-break flow and bed load modelling using HLLC-WAF scheme

Alireza Hosseinzadeh-Tabrizi and Mahnaz Ghaeini-Hessaroeyeh

ABSTRACT

A two-dimensional numerical model predicting flow over a mobile bed has been developed. Governing equations consist of the shallow water equations and the Exner equation. The finite volume method on an unstructured triangular grid was deployed to discretize the governing equations. The local Riemann problem is solved by the Harten, Lax and van Leer–contact (HLLC) method in the interface of the cells and the equations are solved using a fully coupled method. Then the flux modelling has been deployed by the total variation diminishing (TVD) version of the weighted average flux (WAF) scheme. The model was verified by comparison of the results and available experimental data for dam-break flow, in a laboratory test, via a channel with sudden enlargement and erodible bed conditions. Comparison of these two sets of results shows that increasing the accuracy of flux modelling caused the model results to have a reasonable agreement with the experimental data.

Key words | finite volume method, HLLC method, mobile bed, shallow water equations, TVD-WAF method

Alireza Hosseinzadeh-Tabrizi (corresponding author)
Mahnaz Ghaeini-Hessaroeyeh
Department of Civil Engineering, Faculty of Engineering,
Shahid Bahonar University of Kerman,
P.O. Box 76169133,
Kerman,
Iran
E-mail: *alireza.tabrizi@eng.uk.ac.ir*

INTRODUCTION

Dam-break flows usually propagate along rivers and floodplains, where huge and sudden fluid flow occurs with sediment transport and bed changes (Xia *et al.* 2010); however, a flow model is usually applied for flow over a fixed bed. Nonetheless, remarkable models have been developed which are capable of simulating morphological evolution of the bed.

In recent years, applications of the schemes based on the finite volume method (FVM) in simulating dam-break phenomena have been increased. Especially, the upwind Godunov-type schemes via the FVM are very popular due to their robustness and accuracy in capturing discontinuities. A comparison of the performance of upwind schemes based on FVM, namely the Osher scheme, Roe scheme, Harten, Lax and van Leer (HLL) scheme and Harten, Lax and van Leer–contact (HLLC) scheme, was performed by Erduran *et al.* (2002). They investigated and compared the accuracy, applicability, efficiency and stability of different Riemann solvers in the finite volume shallow flow model. According to the mentioned study, it is recommended that the HLLC Riemann solver is suitable for all kinds of applications. Many researchers have developed and customized schemes based on FVM.

One of the first researchers is Patankar. Patankar & Spalding (1972) used FVM in order to find a numerical solution for the heat transfer equations. Then De Vriend (1987) worked on the theoretical basis of the behaviour of two-dimensional sediment transport and morphological models. Struiksma (1985) developed a two-dimensional sediment transport model to simulate large-scale bed change. Van-Rijn (1987) developed a two-dimensional vertical model for predicting morphological changes via laboratory testing. Hirsch (1988) employed the discretization of the integral form of conservative equations across a discontinuity. Shimizu & Itakura (1989) developed a two-dimensional bed load transport model for alluvial channels. Chaudhry (1993) used shock capturing methods for simulating one-dimensional open-channel flows. Kassem (1996) developed a two-dimensional bed load sediment transport model for straight and meandering channels. Anastasiou & Chan (1997) provided a model based on the shallow water equations using FVM on unstructured triangular meshes. Valiani *et al.* (2002) utilized the conservative form of shallow water equations with a Godunov-type scheme. Yoon & Kang (2004) used the HLL approximate Riemann solver and multidimensional slope-limiting approach in some test cases. Cao *et al.* (2004) presented a one-dimensional dam-break model considering erodible sediment beds. Loukili & Soulaimani (2007) developed a model

doi: 10.2166/wst.2015.324

using weighted average flux (WAF) approximation for modelling fluxes at the cell interfaces on an unstructured grid. Goutiere *et al.* (2008) investigated eigenvalues of a complete system (flow and sediment transport) and eigenvalues of the water phase only in a one-dimensional model. Iervolino *et al.* (2010) surveyed the effect of sudden enlargement of the channel on simulation of dam-break with a mobile bed. Benkhaldoun *et al.* (2012) and also Murillo & Garcia-Navarro (2010) used FVM to solve a coupled model of water flow and sediment transport and bed evolution. Soares-Frazao & Zech (2010) introduced a new approach consisting of estimating wave speeds considering sediment properties in two-dimensional shallow-water flow and erodible bed conditions. Li *et al.* (2013) developed a morphological model using a fully coupled, total variation diminishing upwind-biased centred scheme. Hsu *et al.* (2014) presented a model for surveying dam-break wave propagation and its implications for sediment erosion.

In this study, a two-dimensional flow model over a mobile bed has been developed. The HLLC scheme with novel wave speed proposed by Soares-Frazao & Zech (2010) is selected for flux modelling in the cell interfaces. To achieve second-order accuracy, the WAF method is employed, which was introduced by Toro (1999). According to Godunov's theorem, schemes with high-order accuracy generate spurious oscillations near large gradients of the solution. The WAF method is used with a flux amplifying function for avoiding the mentioned problem and getting a non-linear total variation diminishing (TVD) scheme of second-order accuracy.

In the following part, the governing shallow water equations are described, and then the details of the development of the numerical model are presented. The model is applied for dam-break flow in a channel with a sudden enlarged section and erodible bed conditions.

METHODS

Governing equations

The shallow water equations express the mass and momentum conservation of flow and the Exner equation describes mass conservation of the bed material (Graf & Altinakar 1998) and expresses the variation of the bed level following erosion or deposition. In the present model, sediment transport is characterized by bed load only, thus the role of suspended load has been ignored, and then the governing equations can be written as the following relation (Soares-Frazao & Zech 2010)

$$\frac{\partial U}{\partial t}+\frac{\partial F(U)}{\partial x}+\frac{\partial G(U)}{\partial y}=S \tag{1}$$

where

$$U=\begin{bmatrix}h\\uh\\vh\\z_b\end{bmatrix}=\begin{bmatrix}h\\q_x\\q_y\\z_b\end{bmatrix},\ F=\begin{bmatrix}q_x\\{q_x}^2+gh^2/2\\q_xq_y/h\\q_{s,x}/(1-e_0)\end{bmatrix}=\begin{bmatrix}q_x\\\sigma_x\\\mu_{xy}\\q_{s,x}/(1-e_0)\end{bmatrix}$$

$$G=\begin{bmatrix}q_y\\{q_y}^2+gh^2/2\\q_xq_y/h\\q_{s,y}/(1-e_0)\end{bmatrix}=\begin{bmatrix}q_y\\\sigma_y\\\mu_{xy}\\q_{s,y}/(1-e_0)\end{bmatrix},\ S=\begin{bmatrix}0\\gh(s_{0,x}-s_{f,x})\\gh(s_{0,y}-s_{f,y})\\0\end{bmatrix} \tag{2}$$

where t is the time, x and y the space coordinates, g the gravitational acceleration, h the water depth, u and v the depth-averaged velocity components, respectively, in the x and y directions, q_x and q_y the unit discharge components, z_b the erodible bed elevation, $q_{s,x}$ and $q_{s,y}$ the components of the sediment transport rate per unit width and e_0 the bed porosity.

In the source term S, $S_{0,x}$ and $S_{0,y}$ are the bed slopes in the x and y directions, respectively, and $S_{f,x}$, $S_{f,y}$ the friction slope components. The friction slope is calculated using the Manning formula. The sediment transport rate q_s is calculated using a suitable relation. The Meyer-Peter and Müller-type formula with ad hoc coefficients is used (Ribberink 1998) for sediment transport calculation because it appeared well suited and reasonable to the experimental test with an enlargement section in our study. The Ribberink formula is as follows:

$$q_s(q,h)=11\sqrt{g(s-1)d_{50}^3}(\max\,(0,\tau_*-\tau_{*c}))^{1.65} \tag{3}$$

where s is the relative density of sediment, d_{50} is a representative grain diameter, τ_* denotes the non-dimensional bed shear stress and τ_{*c} the non-dimensional critical bed shear stress. It is thought that sediment starts to move when $\tau_*\geq\tau_{*c}$ ($\tau_{*c}\simeq 0.047$). The non-dimensional bed shear stress is calculated as follows:

$$\tau_*=\frac{n^2q^2}{(s-1)d_{50}h^{7/3}} \tag{4}$$

where $q=\sqrt{q_x^2+q_y^2}$ and n is the Manning friction coefficient.

In schemes based on FVM, the fluxes are calculated across the cell interfaces; so, using the rotational invariance property in the direction normal to the considered interface, the variables are described in a local coordinate system (x_n, y_t) related to the interface. The local coordinate system for an unstructured triangle mesh is shown in Figure 1.

The eigenstructure of the system analysed for the equations written in these local coordinates (x_n, y_t) and the friction source terms were neglected because of having inconsiderable influence on wave-propagation properties. After the rotation from the system (x, y) to the system (x_n, y_t), the system of Equation (1) becomes (Soares-Frazao & Zech 2010):

$$\frac{\partial \bar{U}}{\partial t}+\frac{\partial F(\bar{U})}{\partial x_n}+H(\bar{U})\frac{\partial \bar{U}}{\partial x_n}+\frac{\partial G(\bar{U})}{\partial y_t}+k(U)\frac{\partial \bar{U}}{\partial y_t}=0 \tag{5}$$

where

$$\bar{U}=\begin{bmatrix} h \\ q_n \\ q_t \\ z_b \end{bmatrix}, \mathrm{F}(\bar{U})=\begin{bmatrix} q_n \\ {q_n}^2+gh^2/2 \\ q_n q_t/h \\ q_{s,n}/(1-\varepsilon_0) \end{bmatrix}=\begin{bmatrix} q_n \\ \sigma_n \\ \mu_{nt} \\ q_{s,n}/(1-\varepsilon_0) \end{bmatrix}$$

$$\mathrm{G}(\bar{U})=\begin{bmatrix} q_t \\ q_n q_t/h \\ {q_t}^2+gh^2/2 \\ q_{s,t}/(1-\varepsilon_0) \end{bmatrix}=\begin{bmatrix} q_t \\ \mu_{nt} \\ \sigma_t \\ q_{s,t}/(1-\varepsilon_0) \end{bmatrix}$$

$$H(\bar{U})=\begin{pmatrix} 0 & 0 & 0 & 0 \\ 0 & 0 & 0 & gh \\ 0 & 0 & 0 & 0 \\ 0 & 0 & 0 & 0 \end{pmatrix} K(\bar{U})=\begin{pmatrix} 0 & 0 & 0 & 0 \\ 0 & 0 & 0 & 0 \\ 0 & 0 & 0 & gh \\ 0 & 0 & 0 & 0 \end{pmatrix} \tag{6}$$

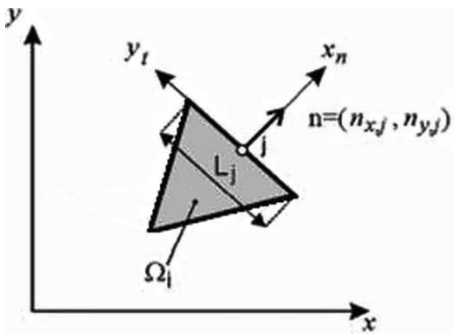

Figure 1 | Local coordinate system for an unstructured triangle mesh (Soares-Frazao & Zech 2010).

As was mentioned before, according to the basic principle of the finite volume schemes, only the terms in the normal direction x_n are considered. For analysis of the wave-propagation properties of the system, Equation (5) is transformed to the following equation:

$$\frac{\partial \bar{U}}{\partial t}+\frac{\partial F(\bar{U})}{\partial x_n}+H(\bar{U})\frac{\partial \bar{U}}{\partial x_n}=0 \tag{7}$$

Equation (7) corresponds to the so-called augmented one-dimensional problem (Toro 1999) that is identical to a split multidimensional system in Cartesian coordinates. The eigenvalue analysis was carried out completely from Equation (7) and the validation process of the approximate analytical expression for the eigenvalues was performed accurately (Soares-Frazao & Zech 2010). Some corrections are implemented because of using Ribberink's formula (Ribberink 1998) instead of the Meyer-Peter and Müller original formula. Then the eigenvalues resulting from the mentioned process are in two types as follows (Soares-Frazao & Zech 2010):

$$\begin{cases} \lambda_1=\left(u_n-c-\sqrt{(u_n-c)^2-\dfrac{4c^2(a_1+a_3v_t)}{u_n+c}}\right) \\ \lambda_2=\left(u_n-c+\sqrt{(u_n-c)^2-\dfrac{4c^2(a_1+a_3v_t)}{u_n+c}}\right) \\ \lambda_3=u_n \\ \lambda_4=u_n+c \end{cases} \tag{8}$$

$$\begin{cases} \lambda_1=\left(u_n-c-\sqrt{(u_n-c)^2+4a^2c^2}\right) \\ \lambda_2=\left(u_n-c+\sqrt{(u_n-c)^2+4a^2c^2}\right) \\ \lambda_3=u_n \\ \lambda_4=u_n+c \end{cases} \tag{9}$$

where $q_{s,n}$ is the sediment transport rate in the normal direction and calculated by the following relations:

$$q_{s,n}=11\sqrt{g(s-1)d_{50}^3}\left(\frac{n^2q_n(q_n^2+q_t^2)^{1/2}}{(s-1)d_{50}h^{7/3}}-\tau_{*c}\right)^{1.65} \tag{10}$$

$$a_1=\frac{1}{(1-\varepsilon_0)}\left(\frac{\partial q_{s,n}}{\partial h}\right), a_2=\frac{1}{(1-\varepsilon_0)}\left(\frac{\partial q_{s,n}}{\partial q_n}\right),$$
$$a_3=\frac{1}{(1-\varepsilon_0)}\left(\frac{\partial q_{s,n}}{\partial q_t}\right), c=\sqrt{gh} \tag{11}$$

$$\frac{\partial q_{s,n}}{\partial h} = -18.15\sqrt{g(s-1)d_{50}^3}\left(\frac{n^2 q_n (q_n^2+q_t^2)^{1/2}}{(s-1)d_{50}h^{7/3}} - \tau_{*c}\right)^{0.65} 7/3\frac{n^2 q_n (q_n^2+q_t^2)^{1/2}}{(s-1)d_{50}h^{10/3}}$$

$$\frac{\partial q_{s,n}}{\partial q_n} = 18.15\sqrt{g(s-1)d_{50}^3}\left(\frac{n^2 q_n (q_n^2+q_t^2)^{1/2}}{(s-1)d_{50}h^{7/3}} - \tau_{*c}\right)^{0.65} \frac{n^2}{(s-1)d_{50}h^{7/3}}(q_n^2+q_t^2)^{1/2}\left(1+\frac{q_n^2}{q_n^2+q_t^2}\right)$$

$$\frac{\partial q_{s,n}}{\partial q_t} = 18.15\sqrt{g(s-1)d_{50}^3} \left(\frac{n^2 q_n (q_n^2+q_t^2)^{1/2}}{(s-1)d_{50}h^{7/3}} - \tau_{*c}\right)^{0.65} \frac{n^2}{(s-1)d_{50}h^{7/3}} \frac{q_n q_t}{(q_n^2+q_t^2)^{1/2}} \quad (12)$$

As was mentioned before, the validity of two types of eigenvalues has been checked by comparison with the exact eigenvalues (Soares-Frazao & Zech 2010). But expressions in Equation (8) appear less convenient than those in Equation (9), because there is a singular point when $u_n + c = 0$, although both types in the present research, with some programming consideration, are used.

The HLL approximate Riemann solver

It is shown in Figure 2 the wave structure in the HLL approach. The numerical flux of HLL is evaluated as follows (Toro 2000):

$$F_{i+1/2} = \begin{cases} F_L & \text{if } \lambda_L \geq 0 \\ F^{\text{hll}} = \dfrac{\lambda_R F_L - \lambda_L F_R + \lambda_R \lambda_L (U_R - U_L)}{\lambda_R - \lambda_L} & \text{if } \lambda_L \leq 0 \leq \lambda_R \\ F_R & \text{if } \lambda_R \leq 0 \end{cases} \quad (13)$$

where λ_L and λ_R are the smallest and largest signal velocities in the solution of the Riemann problem with data $U_L = U_i^n$, $U_R = U_{i+1}^n$ and the corresponding fluxes are

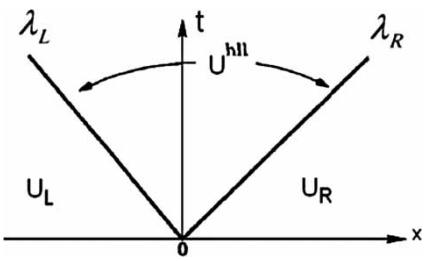

Figure 2 | Wave structure of HLL Riemann solver (Toro 2000).

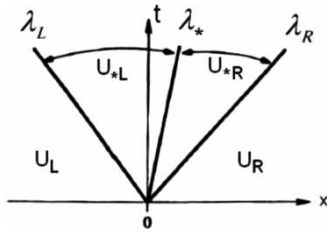

Figure 3 | Wave structure of HLLC Riemann solver (Toro 2000).

calculated by following relations:

$$F_L = F(U_L),\ F_R = F(U_R)$$

The HLLC approximate Riemann solver

The HLLC scheme is a modification of the HLL scheme described in the previous section, whereby the missing contact and shear waves are restored. The wave structure in the HLLC approach is shown in Figure 3.

The simpler version of the HLLC solver is used for the approximate Godunov method as follows. The third component of flux ($F_{i+1/2}$) can be expressed in terms of the first component and the variable v (shear wave velocity), that is $F^3 = F^1 v$. Then retaining the HLL fluxes for the first two components of the flux, the third component is as follows (Toro 2000):

$$F_{i+1/2}^3 = \begin{cases} F_{i+1/2}^1 \, v_L & \text{if } u_* \geq 0 \\ F_{i+1/2}^1 \, v_R & \text{if } u_* < 0 \end{cases} \quad (14)$$

Then the HLL fluxes are suitable for the first and second components of the flux.

In the HLLC solver, the wave speed was estimated without considering the properties of bed material. Therefore, these properties need to be considered to improve the wave speed estimation.

Modified HLLC scheme for the fluxes in the case with sediments

The HLLC scheme is used, with a modification to introduce the sediment-related characteristic in the expression for the sediment transport rate across a cell interface. Owing to the small celerity of sediment-related information (λ_2 in the subcritical case, and λ_1 in the supercritical case), the classical HLLC flux formulation has been used for the first three components of the intercell flux F^*. According to the

research of Soares-Frazao & Zech (2010) the HLLC intercell flux in the case with sediments is calculated by the following relation:

$$F^* = \begin{bmatrix} q_n^* \\ \sigma_n^* \\ \mu_{nt}^* \\ q_{s,n}^*/(1-\varepsilon_0) \end{bmatrix} \tag{15}$$

where q_n^* and σ_n^* are mass flux and momentum flux in the normal direction and μ_{nt}^* is momentum flux in the transverse direction. Then the flux expressions are evaluated as follows (Soares-Frazao & Zech 2010):

$$q_n^* = \frac{\lambda^+ q_{n,L} - \lambda^- q_{n,R} + \lambda^+\lambda^-(z_{w,R} - z_{w,L})}{\lambda^+ - \lambda^-} \tag{16}$$

$$\sigma_n^* = \frac{\lambda^+ \sigma_{n,L} - \lambda^- \sigma_{n,R} + \lambda^+\lambda^-(q_{n,R} - q_{n,L})}{\lambda^+ - \lambda^-} \tag{17}$$

where z_w is the water level and

$$\lambda^+ = \min(\lambda_{1,L}, \lambda_{1,R}),\ \lambda^- = \max(\lambda_{4,L}, \lambda_{4,R}) \tag{18}$$

$$\mu_{nt} = \begin{cases} v_{t,L} & \text{if } u^* \geq 0 \\ v_{t,R} & \text{if } u^* < 0 \end{cases} \tag{19}$$

Finally, the sediment flux in the normal direction is (Soares-Frazao & Zech 2010):

$$q_{s,n}^* = \frac{\lambda_s^+ q_{s,L} - \lambda_s^- q_{s,R} + \lambda_s^+\lambda_s^-(z_{b,R} - z_{b,L})}{\lambda_s^+ - \lambda_s^-} \tag{20}$$

$$\lambda_s^+ = \min(\lambda_{1,L}, \lambda_{1,R}),\ \lambda_s^- = \max(\lambda_{2,L}, \lambda_{2,R}) \tag{21}$$

The waves speed λ_s^+ andλ_s^- are related to the minimum and maximum wave speeds corresponding to the sediment movement at the interface (Soares-Frazao & Zech 2010).

Formulations of the WAF method

The WAF approach for obtaining second-order extensions of the Godunov first-order upwind method has its origins in the random flux method (Toro 1999). WAF is a deterministic approach and has two versions. In the first version the intercell flux is an integral average of the physical flux across the full structure of the solution of a local Riemann problem. In the second version, an average state is computed, and the intercell flux, $F_{i+1/2}$, resulted from evaluating the physical flux F at this state (Toro 1999).

The original version of WAF

The WAF flux is given as (Toro 1999):

$$F_{i+1/2} = \frac{1}{\Delta x}\int_{-(1/2)\Delta x}^{(1/2)\Delta x} F\left(U_{i+1/2}\left(x, \frac{\Delta t}{2}\right)\right) dx \tag{22}$$

where $U_{i+1/2}(x, t)$ is the solution of the Riemann problem with piece-wise constant data U_i^n, U_{i+1}^n at the interface position. The solution structure of the Riemann problem is shown in Figure 4.

There are three waves, λ_L, λ_* and λ_R, that separate four constant states: U_i^n, $U_{*\mathrm{L}}$, $U_{*\mathrm{R}}$ and U_{i+1}^n. Figure 5 shows the evaluation of the integral average in Equation (22), for a wave structure assumed to contain no rarefaction waves. By setting

$$U^{(1)} = U_i^n;\quad U^{(2)} = U_{*\mathrm{L}};\quad U^{(3)} = U_{*\mathrm{R}};\quad U^{(4)} = U_{i+1}^n \tag{23}$$

the following relation is obtained:

$$F_{i+1/2} = \sum_{k=1}^{N+1} \beta_k F_{i+1/2}^{(k)} \tag{24}$$

where $F_{i+1/2}^{(k)} = F(U^{(k)})$, N is the number of waves in the solution of the Riemann problem and β_k, $k = 1, \ldots, 4$ are the

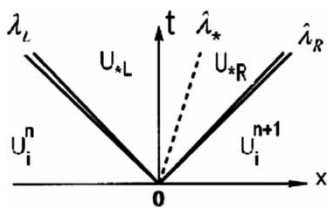

Figure 4 | Solution structure of the Riemann problem with data U_i^n, U_i^{n+1} (Toro 1999).

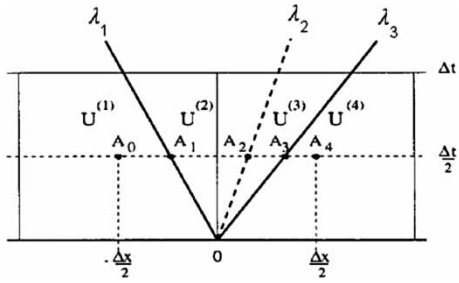

Figure 5 | Evaluation of the WAF intercell flux (Toro 1999).

normalized lengths of the segments A_{k-1}, A_k

$$\beta_k = \frac{|A_{k-1}A_k|}{\Delta x} \tag{25}$$

In terms of the wave speeds λ_k, the weights are (Toro 1999):

$$\beta_k = \frac{1}{2}(c_k - c_{k-1}), \quad c_k = \frac{\Delta t \lambda_k}{\Delta x}, \quad c_0 = -1, \quad c_{N+1} = 1 \tag{26}$$

where c_k is the Courant number for wave k of speed λ_k. The alternative form of WAF flux is obtained by the substitution of β_k from the Equation (26) into the Equation (24).

$$F_{i+1/2} = \frac{1}{2}(F_i + F_{i+1}) - \frac{1}{2}\sum_{k=1}^{N} c_k \Delta F^{(k)}_{i+1/2} \tag{27}$$

where $\Delta F^{(k)}_{i+1/2} = F^{(k+1)}_{i+1/2} - F^{(k)}_{i+1/2}$ is the flux jump across wave k of the Courant–Friedrichs–Lewy (CFL) number c_k. In the CFL condition, Δx is taken to be the minimum distance between two volume centres, but at boundaries, the distance between the centre of the element and the volume centre is used.

TVD version of WAF schemes

According to Godunov's theorem, spurious oscillations near high gradient regions are to be expected in WAF schemes; so the TVD version of WAF should be used to prevent the oscillations. The principle of TVD is to amplify the wave speeds in the solution of the local Riemann problem; this is achieved by multiplying the Courant number c_k by an amplifying function A_k. Thus oscillation-free WAF flux is obtained by the following relation (Toro 1990):

$$F_{i+1/2} = \frac{1}{2}(F_i + F_{i+1}) - \frac{1}{2}\sum_{k=1}^{N} A_k c_k \Delta F^{(k)}_{i+1/2} \tag{28}$$

The amplifying function (also called limiter function) $A_k = A_k(U)$ is a function of the flow features. Three limiters which are applied in the present model are presented below (Toro 1999):

$$(\text{van Leer})A_k = \begin{cases} \dfrac{1}{|c_k|} & \text{if } r \le 0 \\ \dfrac{1-[1-2r(1-|c_k|)/(1+r)]}{|c_k|} & \text{if } r \ge 0 \end{cases}$$

$$(\text{Superbee})A_k = \begin{cases} \dfrac{1-2(1-|c_k|)}{|c_k|} & \text{if } r \ge 2 \\ \dfrac{1-(1-|c_k|)r}{|c_k|} & \text{if } 1 \le r \le 2 \\ 1 & \text{if } \dfrac{1}{2} \le r \le 1 \\ \dfrac{1-2r(1-|c_k|)}{|c_k|} & \text{if } 0 \le r \le \dfrac{1}{2} \\ \dfrac{1}{|c_k|} & \text{if } 0 \le r \le \dfrac{1}{2} \end{cases}$$

$$(\text{Minbee})A_k = \begin{cases} \dfrac{1}{|c_k|} & \text{if } r \le 0 \\ \dfrac{1-(1-|c_k|)r}{|c_k|} & \text{if } 0 \le r \le 1 \\ 1 & \text{if } r \ge 1 \end{cases} \tag{29}$$

The flow parameter r is calculated as follows (Toro 1999):

$$r = \begin{cases} \dfrac{\Delta Q^{(k)}_{i-1/2}}{\Delta Q^{(k)}_{i+1/2}} & \text{if } c_k \ge 0 \\ \dfrac{\Delta Q^{(k)}_{i+3/2}}{\Delta Q^{(k)}_{i+1/2}} & \text{if } c_k < 0 \end{cases} \tag{30}$$

For the shallow water equations, $Q = h$ for the acoustic waves, $Q = v$ for the contact wave and $Q = z_b$ for the sediment are selected. The notation $\Delta Q^{(k)}_{i+1/2}$ means the jump in Q across the wave k in the Riemann problem with data (U_i, U_{i+1}). Since the waves in the Riemann problem generally travel in different directions one must construct a function A_k for each wave. For instance, in the triangular mesh, the left and right upwind states are computed as the mean value of states in L_{upw1}, L_{upw2}, R_{upw1}, R_{upw2} weighted by their relative areas according to Figure 6.

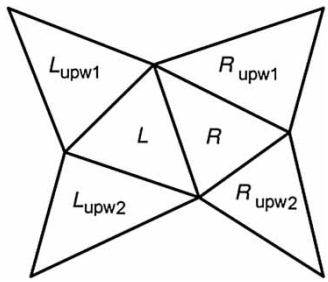

Figure 6 | Schematization of upwind volumes (Loukili & Soulaimani 2007).

Combining HLLC and WAF schemes (HLLC-WAF) in mobile bed conditions

Using a weighted average of HLLC fluxes for the two first components and fourth component and a weighted average of WAF flux itself for the third component with TVD modification, the components of the HLLC-WAF flux are calculated as follows (Loukili & Soulaimani 2007).

For first, second and fourth components:

$$F_{i+1/2}^{WAF} = \frac{1}{2}(F_i + F_{i+1}) - \frac{1}{2}\sum_{k=1}^{N} A_k c_k \Delta F_{i+1/2}^{(k)} \tag{31}$$

For the third component:

$$F_{i+1/2}^{WAF} = \left(\frac{1}{2}(v_i + v_{i+1}) - \frac{1}{2}A_* c_* \Delta v\right) * F_{i+1/2}^{WAF}(1) \tag{32}$$

where v is the tangential velocity in the local coordinates, A_* and c_* are calculated according to contact discontinuity wave velocity. After using well-known amplifying functions, the van Leer function was selected in the present model.

Boundary conditions

For the WAF scheme as the second-order method the application of boundary conditions is fundamentally the same as the Godunov method. The computational domain is assumed which discretized by N cells, so that cells $i = 1, \ldots, N$ lie within the computational domain. Also the Mth cell is assumed to be the boundary cell. For applying boundary conditions two fictitious cells next to each boundary are needed. For the left boundary the fictitious cells are denoted by $i = M-2$ and $i = M-1$ and for the right boundary they are denoted by $i = M+1$ and $i = M+2$. Two types of boundary conditions are discussed.

Transmissive boundary conditions are given by the following relations:

$$\begin{cases} h_{M-1}^n = h_M^n \\ u_{M-1}^n = u_M^n \\ z_{b,M-1}^n = z_{b1}^n \end{cases} \begin{cases} h_{M-2}^n = h_{M+1}^n \\ u_{M-2}^n = u_{M+1}^n \\ z_{b,M-2}^n = z_{b,M+1}^n \end{cases} \begin{cases} h_{M+1}^n = h_M^n \\ u_{M+1}^n = u_M^n \\ z_{b,M+1}^n = z_{b,M}^n \end{cases} \times \begin{cases} h_{M+2}^n = h_{M-1}^n \\ u_{M+2}^n = u_{M-1}^n \\ z_{b,M+2}^n = z_{b,M-1}^n \end{cases} \tag{33}$$

Reflective boundary conditions are given by the following relations:

$$\begin{cases} h_{M-1}^n = h_M^n \\ u_{M-1}^n = -u_M^n \\ z_{b,M-1}^n = z_{bM}^n \end{cases} \begin{cases} h_{M-2}^n = h_{M+1}^n \\ u_{M-2}^n = -u_{M+1}^n \\ z_{b,M-2}^n = z_{b,M+1}^n \end{cases} \begin{cases} h_{M+1}^n = h_M^n \\ u_{M+1}^n = -u_M^n \\ z_{b,M+1}^n = z_{b,M}^n \end{cases} \times \begin{cases} h_{M+2}^n = h_{M-1}^n \\ u_{M+2}^n = -u_{M-1}^n \\ z_{b,M+2}^n = z_{b,M-1}^n \end{cases} \tag{34}$$

where h is the water depth, u is the velocity component in the x or y direction considering boundary direction, z_b is the sediment depth (Toro 1999). In the domain of the test case all of the boundary forms using R_{upw} for the right upwind and L_{upw} for the left upwind side are depicted in Figure 7.

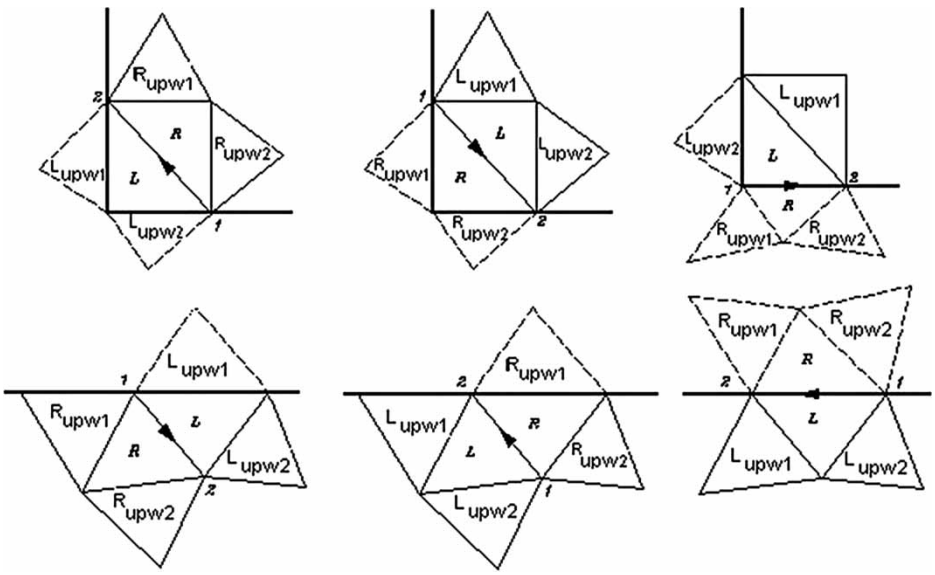

Figure 7 | All possible forms of the boundaries and their relative upwind volumes.

Finite volume numerical model

The present model has been developed using the finite volume method. First, the computational domain is divided into a set of triangular finite volumes. Then the governing equations are integrated over each control volume and the following relation is obtained by applying the divergence theorem:

$$\frac{\partial}{\partial t}\int_{\Omega_i} U\,\mathrm{d}V + \oint_{S_i} F\cdot n\,\mathrm{d}S = \int_{\Omega_I} S\,\mathrm{d}V \tag{35}$$

where n is the outward-directed unit vector normal to the boundary S_i and F is the flux vector. The integrand $F{\cdot}n$ is the normal flux across a surface. Equation (35) implies that the time rate of change in U inside a control volume depends on the total flux through the surface of the volume plus the sum of sources within the volume. To facilitate solution of Equation (35) in this paper the approach of Zoppou & Roberts (2000) is followed so the rotation matrix T is as below:

$$T = \begin{bmatrix} 1 & 0 & 0 & 0 \\ 0 & n_x & n_y & 0 \\ 0 & -n_y & n_x & 0 \\ 0 & 0 & 0 & 1 \end{bmatrix} \tag{36}$$

Using the rotational invariance property of the two-dimensional shallow water equations, then

$$F(U)\cdot n = F(TU) \tag{37}$$

Conversely, by applying Equation (37), Equation (35) is transformed into:

$$U_i^{n+1} = U_i^n - \frac{\Delta t}{\Omega_i}\sum_{j=1}^{nb} T_j^{-1} F_j^*(\bar{U}_j) L_J + S_{F,i}\Delta t \tag{38}$$

where Ω is the cell-base area, L_j the j -interface length and nb the number of cell interfaces (three for triangular cells). As in Equation (5), vectors $\bar{U}$ and $F(\bar{U})$ express U and F in terms of normal and tangential velocity components u_n and v_t, attached to the considered interface. The transformation of coordinates is obtained via rotational matrix T, where n_x and n_y are the components of the outward unit vector normal to the interface:

$$\bar{U} = \begin{bmatrix} h \\ u_n h \\ v_t h \\ z_b \end{bmatrix} = TU = \begin{bmatrix} 1 & 0 & 0 & 0 \\ 0 & n_x & n_y & 0 \\ 0 & -n_y & n_x & 0 \\ 0 & 0 & 0 & 1 \end{bmatrix} \begin{bmatrix} h \\ uh \\ vh \\ z_b \end{bmatrix} \quad S_{F,i} = \begin{bmatrix} 0 \\ S_{f,x} \\ S_{f,y} \\ 0 \end{bmatrix} \tag{39}$$

For the source term $S_{F,i}$, the friction slopes $S_{f,x}$ and $S_{f,y}$ are calculated using the Manning formula as follows:

$$\mathrm{S}_{f,x} = \frac{n^2 u\sqrt{u^2+v^2}}{h^{4/3}} \quad \mathrm{S}_{f,y} = \frac{n^2 v\sqrt{u^2+v^2}}{h^{4/3}} \tag{40}$$

Finally, due to the explicit nature of the scheme, stability is dictated by the CFL condition on the time step Δt (Courant *et al.* 1967).

Test case: dam-break flow in an erodible open channel with a sudden enlarged section

The present model is applied to model dam-break flow in an erodible channel. Palumbo *et al.* (2008) reported an experimental investigation on a model of dam-break flow in an erodible channel with a sudden enlargement. The flow domain consists of an upstream reservoir which has a length of 3 m, and there is a widening from 0.25 m to 0.50 m at 1 m downstream of the gate.

As can be seen in Figure 8, there is an initial sediment layer of 0.1 m all over the flume and the initial water depth is 0.25 m in the reservoir. In the downstream part of the flume, the sediment layer is saturated with water, but there is no water depth above the sediment layer. The sediments consist of coarse sand with median diameter $d_{50} = 1.65$ mm, deposited with a porosity $\varepsilon_0 = 0.42$. At the downstream end of the flume, there is a weir where the crest is at the top level of the sediment layer, so a free outflow occurs. The water level evolution and the final bed topography were recorded at specific points in the flume (Figure 8).

In the present model, the computational domain is divided into 8,035 triangular cells. The triangular grids are shown in Figure 9.

Comparisons between the measurements of Palumbo *et al.* (2008) and the present model results for the water level at different stations and the bed elevation in different sections are shown in Figures 10 and 11 respectively.

RESULTS AND DISCUSSION

Comparing the numerical modelling results at the points U2, U3, U6 and U7 with the experimental test results (EXTR) shows very good convergence at the point U2. The start of the increase in water level, the maximum water level (z_w), the time related to the maximum water level, and the water level related to the end time are generally well

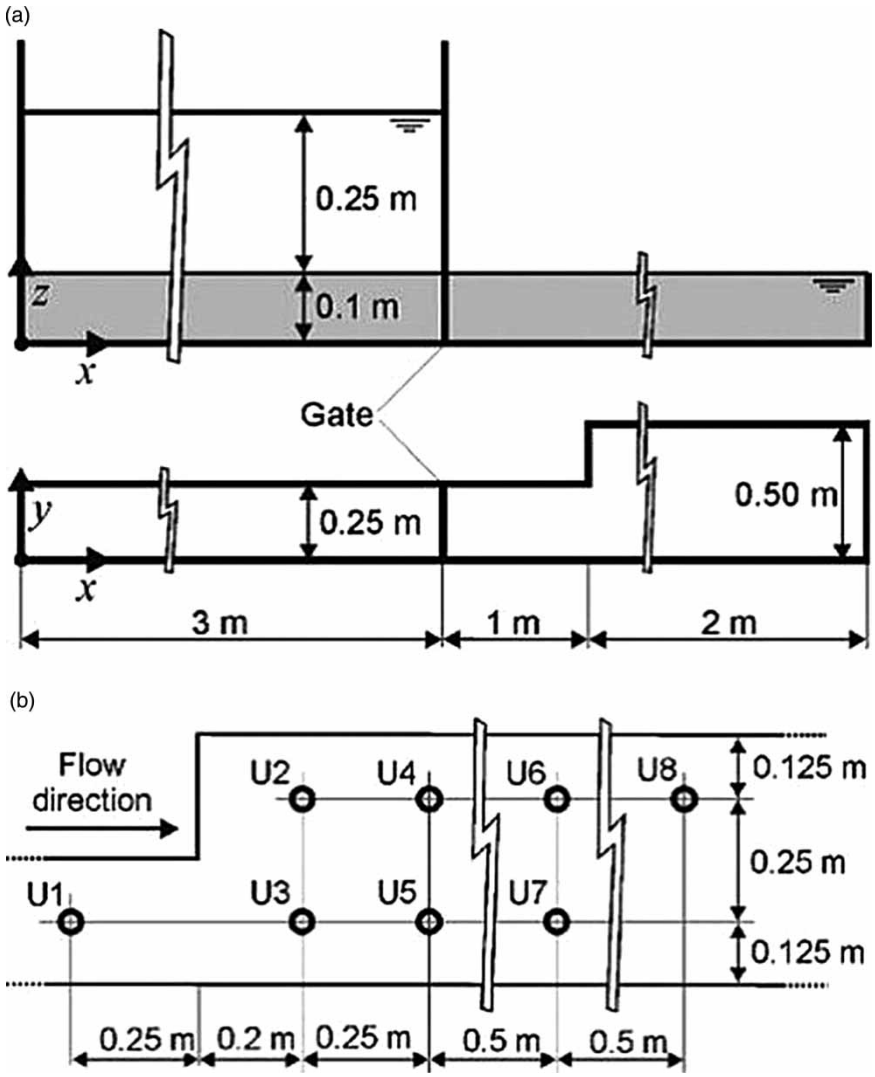

Figure 8 | Experimental set-up: (a) dimensions and initial conditions and (b) location of the measurement points (Soares-Frazao & Zech 2010).

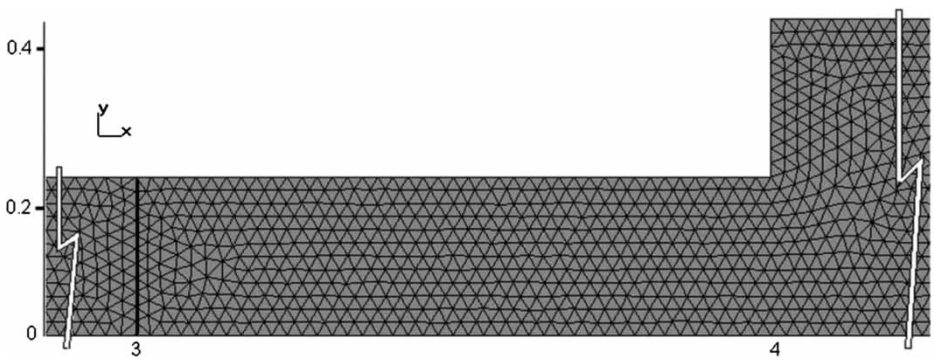

Figure 9 | Triangular grids in the present model.

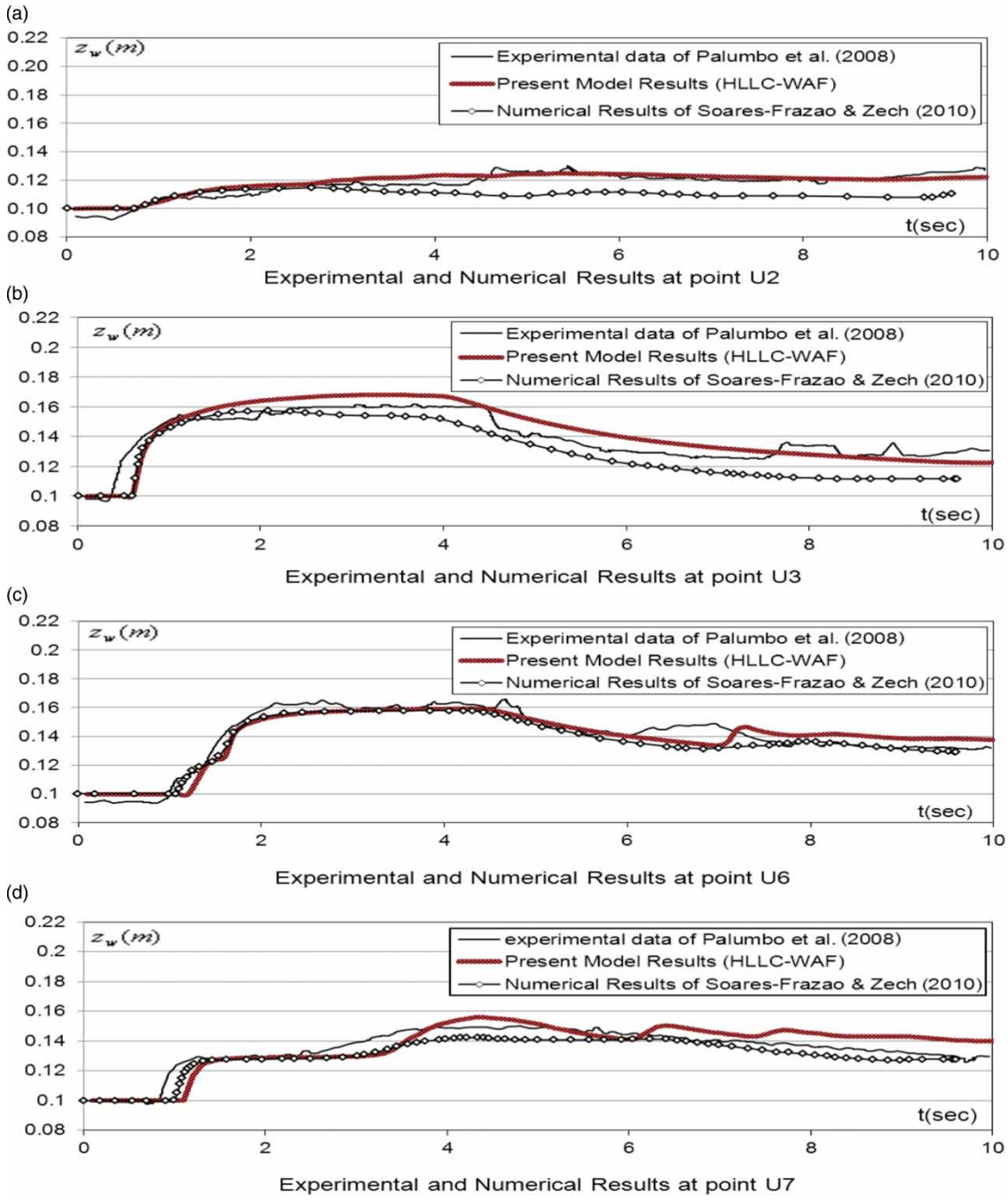

Figure 10 | Comparison of experimental data of Palumbo *et al*. (2008) and the present model results and numerical model of Soares-Frazao & Zech (2010) for water levels at four gauging points: (a) U2 ($x = 4.20$ m; $y = 0.375$ m); (b) U3 ($x = 4.20$ m; $y = 0.125$ m); (c) U6 ($x = 4.95$ m; $y = 0.375$ m); and (d) U7 ($x = 4.95$ m; $y = 0.125$ m).

reproduced by the results of the present model using the HLLC-WAF method.

According to the water level increase after t = 8 sec at the point U2 (Figure 10(a)), the present model result by the TVD-WAF method shows that kind of increase very well. At the point U3 (Figure 10(b)), the increase time of the water level results in the TVD-WAF method is different by about 0.3 sec comparing with EXTR. The maximum water level is a bit higher than EXTR but lowering the water level has been well reproduced as well as the water level related to the end time.

At the point U6 (Figure 10(c)), the shape of the water level increase between $t = 1$ sec and $t = 2$ sec has been well reproduced as well as the maximum water level in the model results by the HLLC-WAF method. Also the shape

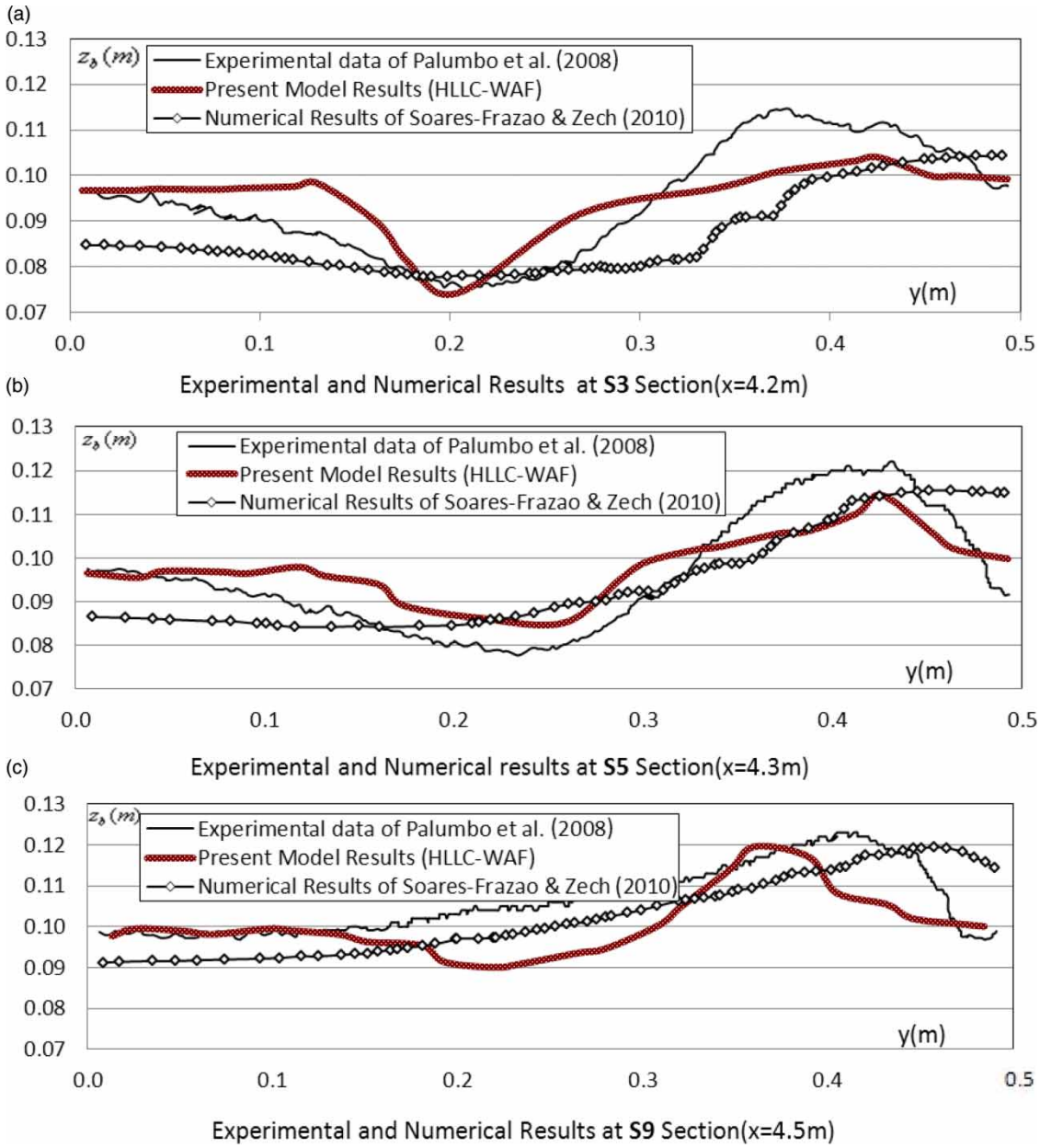

Figure 11 | Comparison of experimental data of Palumbo *et al.* (2008) and the present model results and numerical model of Soares-Frazao & Zech (2010) for bed elevation at cross-sections: (a) S3 ($x = 4.20$ m); (b) S5 ($x = 4.30$ m); and (c) S9 ($x = 4.50$ m).

of the water level increase after $t = 6$ sec is simulated at t = 7 sec due to the influence of the second-order accuracy upwind method which has been employed in the present model.

At the point U7 (Figure 10(d)), the maximum water level has been well simulated. Probably it is resulted from some deviation in predicting bed level. Furthermore, the water level increase shape from the results of the TVD-WAF method is similar to EXTR.

Comparisons between measurements of Palumbo *et al.* (2008) and the present model results for bed elevation at different sections are shown in Figure 11. As is shown in Figure 11, the morphological change on the bed is rather well simulated at sections S3, S5 and S9.

At the section S3 (Figure 11(a)), the shape of the bed profile change in the model results is rather near to EXTR and the maximum and minimum level in the profile is well reproduced at $y = 0.2$ m and $y = 0.42$ m, considering

the fact that the same coordinates in the test are $y = 0.22$ m and $y = 0.38$ m approximately. Only in two parts ($y = 0.13$ m and $y = 0.25$ m) are there little unexpected bed increases that are not considerable because of the good general shape of the bed profile in the numerical simulation at the section S3.

Also at the section S5 (Figure 11(b)) the shape of the bed profile is very well reproduced and compared to S3 and S9. The results of the present model in this section are the best ones comparing to the maximum and minimum bed level in the EXTR. So the values of the maximum and minimum bed level are approximately equal to the EXTR and they are located at $y = 0.23$ m and $y = 0.44$ m for the both numerical and experimental results.

At the section S9 (Figure 11(c)) general convergence of the shape of the bed profile between the numerical and experimental results is valid and discrepancies between $y = 0.15$ m and $y = 0.3$ m may result from the other effects of the flow that are not considered in the present model, such as the effect of secondary currents and changing of flow velocity in the vertical profile of the channel. Nonetheless, relatively acceptable predictions of flow in the present model results compared to the experimental results are provided.

For further evaluating use of the second-order accuracy TVD-WAF scheme in conjunction with the HLLC scheme, comparison of the present model results with the numerical results of Soares-Frazao & Zech (2010) are presented for the water level and sediment bed level in Figures 10 and 11.

According to the present model results, the complicated pattern of water level has been predicted better by the TVD-WAF method than by the HLLC method. The comparison shows that the results of the HLLC scheme are diffusive and smooth compared to the present model results. Because the HLLC method has first-order accuracy, the results of the HLLC method underestimate the water level and also the bed elevation. The HLLC-WAF scheme indicates better results in view of the convergence between numerical and experimental results. There is an improvement in the results of the HLLC-WAF scheme; however, there are discrepancies between the present model results and EXTR.

CONCLUSIONS

A two-dimensional flow model over a mobile bed has been developed. The governing equations are solved in a coupled approach. The model is based on the finite volume method using a second-order approximate Riemann solver. The TVD version of the WAF scheme in conjunction with the HLLC scheme is capable of simulating changes in the water surface and morphology in the present model. Also the novel analysis of eigenvalues proposed by Soares-Frazao and Zech has been applied. It was successful because of utilization of sediment properties aimed at calculating the eigenvalues and also maximum wave speeds. Furthermore, application of the Ribberink formula for the sediment bed load presents suitable results for the flow over a mobile bed. Finally, the present model is applied for modelling dam-break flow over a mobile bed in a channel with sudden enlargement. Comparison of the model results to the experimental data and the result of the HLLC model shows that the present model can predict better the complicated water level and bed elevation than can the HLLC model. However, there are discrepancies between the present model results and experimental data especially in the bed elevation. The model results might improve by using other formulas for bed changes and considering the effect of three-dimensional flow.

REFERENCES

Anastasiou, K. & Chan, C. T. 1997 Solution of the 2D shallow water equations using the finite volume method on unstructured triangular meshes. *International Journal for Numerical Methods in Fluids* **24**, 1225–1245.

Benkhaldoun, F., Saria, S. & Seaid, M. 2012 A flux-limiter method for dam-break flows over erodible sediment beds. *Journal of Applied Mathematical Modeling* **36** (10), 4847–4861.

Cao, Z., Pender, G., Wallis, S. & Carling, P. 2004 Computational dam-break hydraulics over erodible sediment bed. *Journal of Hydraulic Engineering* **130** (7), 689–703.

Chaudhry, M. H. 1993 *Open-Channel Flow*. Prentice-Hall, Englewood Cliffs, New Jersey, USA.

Courant, R., Friedrichs, K. & Lewy, H. 1967 On the partial difference equations of mathematical physics. *IBM Journal* **11**, 215–234.

De Vriend, H. J. 1987 2DH mathematical modeling of morphological evolutions in shallow water. *Coastal Engineering* **11**, 1–27.

Erduran, K. S., Kutija, V. & Hewett, C. 2002 Performance of finite volume solutions to the shallow water equations with shock-capturing schemes. *International Journal for Numerical Methods in Fluids* **40** (10), 1237–1273.

Goutiere, L., Soares-Frazão, S., Savary, C., Laraichi, T. & Zech, Y. 2008 One-dimensional model for transient flows involving bed-load sediment transport and changes in flow regimes. *Journal of Hydraulic Engineering* **134** (6), 726–735.

Graf, W. H. & Altinakar, M. S. 1998 *Fluvial Hydraulics: Flow and Transport Processes in Channels of Simple Geometry*. Wiley, Chichester, UK.

Hirsch, C. 1988 *Numerical Computation of Internal and External Flows, Fundamentals of Numerical Discretization*. Wiley, Chichester, UK.

Hsu, H., Hsu, T., Torres-Freyermuth, A., Hwung, H. & Kuo, P. 2014 On dam-break wave propagation and its implication to sediment erosion. *Journal of Hydraulic Research* **52** (2), 205–218.

Iervolino, M., Leopardi, A., Soares-Frazao, S., Swartenbroekx, C. & Zech, Y. 2010 2D-H numerical simulation of dam-break flow on mobile bed with sudden enlargement, *International Conference on Fluvial Hydraulics (River Flow 2010)*.

Kassem, A. A. 1996 *Modeling of Sediment Transport in Unsteady Two-Dimensional Open-Channel Flows*, PhD Thesis, Washington State University, Pullman, WA, USA.

Li, W., de Vriend, H. J., Wang, Z. & Maren, V. D. S. 2013 Morphological modeling using a fully coupled, total variation diminishing upwind-biased centered scheme. *Journal of Water Resources Research* **49**, 1–19.

Loukili, Y. & Soulaimani, A. 2007 Numerical tracking of shallow water waves by the unstructured finite volume WAF approximation. *International Journal for Computational Methods in Engineering Science and Mechanics* **8**, 1–14.

Murillo, J. & Garcia-Navarro, P. 2010 An Exner-based coupled model for two-dimensional transient flow over erodible bed. *Journal of Computational Physics* **229** (23), 8704–8732.

Palumbo, A., Soares-Frazao, S., Goutiere, L., Pianese, D. & Zech, Y. 2008 Dam-break flow on mobile bed in a channel with a sudden enlargement. *International Conference on Fluvial hydraulics, Cesme*, **1**, 645–654.

Patankar, S. V. & Spalding, D. B. 1972 A calculation procedure for heat, mass and momentum transfer in three-dimensional parabolic flows. *International Journal of Heat and Mass Transfer* **15**, 1787–1806.

Ribberink, J. S. 1998 Bed-load transport for steady flows and unsteady oscillatory flows. *Coastal Engineering Journal* **34**, 59–82.

Shimizu, Y. & Itakura, T. 1989 Calculation of bed variation in alluvial channels. *Journal of Hydraulic Engineering* **115** (3), 367–384.

Soares-Frazao, S. & Zech, Y. 2010 HLLC scheme with novel wave-speed estimators appropriate for two-dimensional shallow-water flow on erodible bed. *International Journal for Numerical Methods in Fluids* **66**, 1019–1036.

Struiksma, N. 1985 Prediction of 2-D bed topography in rivers. *Journal of Hydraulic Engineering* **111** (8), 1169–1182.

Toro, E. F. 1990 *Riemann Problem and the WAF Method for the Two-Dimensional Shallow Water Equations*. Report Number 9005, Department of Aerospace Sciences, Cranfield University, Cranfield, UK.

Toro, E. F. 1999 *Riemann Solvers and Numerical Methods for Fluid Dynamics: A Practical Introduction*. 2nd edn. Springer, New York.

Toro, E. F. 2000 *Shock-Capturing Methods for Free-Surface Shallow Water*. Wiley, New York.

Valiani, A., Caleffi, V. & Zanni, A. 2002 Case study: Malpasset dam-break simulation using a two-dimensional finite volume method. *ASCE Journal of Hydraulic Engineering* **128** (5), 460–472.

Van Rijn, L. C. 1987 *Mathematical Modeling of Morphological Processes in the Case of Suspended Sediment Transport*, PhD thesis, Civil Engineering Dept, Delft University of Technology, Delft, The Netherlands.

Xia, J., Lin, B., Falconer, R. A. & Wang, G. 2010 Modelling dam-break flows over mobile beds using a 2D coupled approach, *Advances in Water Resources* **33** (2), 171–183.

Yoon, T. H. & Kang, S. K. 2004 Finite volume model for two-dimensional shallow water flows on unstructured grids. *Journal of Hydraulic Engineering* **130**, 678–688.

Zoppou, C. & Roberts, S. 2000 Numerical solution of the two-dimensional unsteady dam break. *Journal of Applied Mathematical Modelling* **24** (7), 457–475.

First received 31 December 2014; accepted in revised form 9 June 2015. Available online 23 June 2015